Damage due to start-stop cycles of turbine runners under high-cycle fatigue

Olivian Savin, Julien Baroth, C. Badina, Sylvie Charbonnier, Christophe Bérenguer

Damage due to start-stop cycles of turbine runners under high-cycle fatigue

O. Savin[1,2,3], J. Baroth[2], C. Badina[1], S. Charbonnier[3], C. Bérenguer[3]

[1] General Technical Division, Electricité de France, F-3800 Saint Martin le Vinoux, France

*2 Univ. Grenoble Alpes, CNRS, Grenoble INP**, 3SR, F-38000 Grenoble, France*

*3 Univ. Grenoble Alpes, CNRS, Grenoble INP**, Gipsa-Lab, F-38000 Grenoble, France*

Corresponding author: julien.baroth@univ-grenoble-alpes.fr

Abstract:

This study presents a strategy to estimate the extra cost due to start-up and shut-down of hydro turbines under high-cycle fatigue. The principle is to compare estimations of cumulated damages from three elementary sequences representing steady and transient regimes (start and stop cycles) of turbine runners, from in-situ strain measurements. Rainflow cycle-counting is used to extract stress cycles from these three sequences. Fatigue design curves are defined, taking into account design codes, laboratory tests and a probabilistic approach. The analysis of these curves, coupled with the Palmgren-Miner rule, allows estimating damage ratio, i.e. extra costs of start and stop events, through an equivalent number of normal operating hours. This approach is applied to Francis and Pelton runners. Different results are discussed in terms of damage distributions and extra costs of start and stops.

***Keywords**:* start and stop, turbine, high cycle fatigue, Wöhler curve, turbine, rainflow cycle-counting, Palgrem-Miner, damage, Francis runner, Pelton runner

Table 1

Nomenclature.

Sigle	Description	Sigle	Description
EdF	Électricité de France	SS	Start and stop
SRH	EdF Hydraulic reparation service	*S-N* curve	Stress vs Number of load cycles
GE	General Electric	FFT	Fast Fourier Transform
ASME	American Society of Mechanical Engineers	N_{noh}	Number of normal operating Hours
RCC-M	Design and Construction Rules for Mechanical Components	FEM	Finite Element Model

Table 2

Main notations.

Symbol	Parameter	Unit	Symbol	Parameter	Unit
YS, UTS	Yield and ultimate tensile strengths of steel	Pa	E	Young's modulus	Pa
σ	Stress	Pa	ε	Strain	µm/m
σ_a	Applied stress amplitude	Pa	σ_m	Mean stress	Pa
σ_{nom}	Nominal stress amplitude	Pa	$\sigma_{\min}, \sigma_{\max}$	Minimal, maximal stress	Pa
FEL	Fatigue endurance limit	Pa	D	Damage	-
Nr	Number of load cycles to failure (Fatigue life)	-	d_{st}, d_{sp}, d_{sy}	Elementary damages	-
N	Number of load cycles	-	$\Delta t_{st}, \Delta t_{sp}, \Delta t_{sy}$	Durations	-
$\sigma_D(N)$	Endurance limit for N cycles	Pa	t	Time	s
K_t	(Fatigue) stress concentration factor	-	μ, s	Mean, standard deviation	-
R	Stress ratio $\sigma_{min}/\sigma_{max}$	-	CV	Coefficient of variation CV=s/ µ	-

1 Introduction

During the last decades, hydro-power plants have been working with an increasing number of start and stop cycles to balance the electric network. Power fluctuations are generated to integrate new types of energy in the electrical grid, but start and stop cycles events are particularly damaging (Gagnon et al. 2010). As a consequence, estimating the cost incurred by start and stop cycles because of increased damage becomes crucial to develop short and long-term operating strategies.

Start and stop cycles events induce degradation of various mechanical equipments of the plants, such as the turbine, penstock and main shut-off valve. Hydroelectric turbines runners are one of the most expensive components to be potentially repaired (Savin et al. 2020). It is also known that fatigue and cavitation are the two main degradation mechanisms of these runners (Dojčinović et al. 2017, Gagnon et al. 2018), among other failure modes (Liu et al. 2016). Fatigue is often considered as the most difficult to manage, particularly in case of fatigue

cracking (Arsić et al. 2013, Dorji & Ghomashchi, 2014, Liu et al., 2016, Luna-Ramirez et al., 2016).

Our aim in this work is to propose a method to quantify the additional cost due to the increased damage on the runners by fatigue due to the starts and stops. This aim in view, two approaches are used for the fatigue assessment (Balaji Rao et al. 2019). On the one hand, some models are based on crack growth and failure criteria (Susmel, 2008, 2009); crack development can occur on the buckets or blades of the turbine runners (Kokko et al. 2014, Welte 2008), Doujak 2016), Hassanipour (2015), Gagnon et al. 2010). On the other hand, some models are based on the relation between the magnitude of the alternating stress history *vs* the number of cycles to failure (S-N curves) in combination with Palmgren-Miner's damage accumulation rule (Marcouiller & Thibaut, 2015). Aiming to quantify the extra cost of start and stops of in-service turbines, this last kind of models is retained.

The proposed approach is based on the analysis of strain measurements near the critical areas where maximum stresses are concentrated in the stainless-steel runner. The analysis of these measurements is based on the selection of steady-state and transient sequences and on the use of rainflow cycle-counting (Matsuishi & Endo, 1969, Amzallag et al. 1994). From the resulting cycle histograms, damage is estimated using a *S-N* curve (Wöhler curve). Such a model linking the stress history and the number of cycles to failure is an engineering tool used for a long time (Wöhler, 1860), but still various works are developed to properly design it for fatigue life prediction (Susmel et al. 2014, Saga et al. 2020). Particularly, it is crucial to account for the stochastic nature of fatigue damage process (Schijve, 2005). This aim in view, probabilistic *S-N* curves, denoted *P-S-N*, allow accounting for large dispersion of fatigue test data (Gagnon et al. 2013).

In this work, we will discuss both the use of design curves, modified using both *P-S-N* and a regulatory curve, as defined using RCC-M (AFCEN, 2008) or ASME (Chopra & Shack, 2003, ASME, 2013). Then, Palmgren-Miner's law is used to estimate cumulative damage (Marcouiller & Thibaut, 2015), for each transient sequence (start-up and shut-down). Finally, we determine the equivalent number of normal operating hours N_{noh} for each start or stop cycle. Such a number can be estimated from expert judgment. Nilsson & Sjelvgren (1997) suggested that one start and stop is equivalent to 15 hours of normal operation. In the same paper, the value of 50 hours for a start and stop is also reported from Mjølsnes, 1999, found in Bakken, 2002 (see also Bakken & Bjørkvoll 2002, Bureau of Reclamation 2014). Anyhow, these values are not properly justified, and to the best of our knowledge, no scientific publication can be found to present in detail how to estimate N_{noh} from in-situ strain measurements, except in brief

conference communications in French (Jacquemoud, 1994) and in French confidential reports (Ballester 1992, EdF & GE, 2018). It is why we propose in the following to present and develop the approach, specifying all the underlying assumptions.

An instrumented Francis runner has been chosen as an example. Such equipment has been designed to start on Monday and to stop on Friday, but nowadays, the start and stop cycles frequency has been drastically increased. It is then crucial to better quantify the effect of these transient sequences.

The first section of the paper highlights consequences of start and stops on the lifetime of turbine runners. It also briefly reminds usual practice to account for fatigue phenomenon. Then a practical fatigue assessment method is presented, estimating damage ratios due to runners start and stops. Then, the method is applied to Francis runners. Finally, conclusions are drawn, highlighting limits and perspectives of the approach.

2 Problem statement

This section is first focused on turbine runners, undergoing fatigue due to start and stop cycles. Then *S-N* curves classically used for fatigue assessment are introduced. Finally, a discussion about the extra cost due to start-up and shut down operations is proposed.

2.1 Turbine runners under fatigue

Common Francis turbines are composed of a runner band, runner crown and fixed blades (Fig. 1). These constructions are casted using stainless steels in 13-17% Cr martensitic (Buxbaum & Ostermann, 1983), (Sonsino & Dieterich, 1990). Particularly, we will consider 13CR-4Ni (or DIN GX5CrNi 13-4), denoted “13-4 stainless steel” in the following. Runners undergo various several transient phenomena, as pointed out by Huth (2005): unsteady loading conditions can be induced by out of phase synchronization during start-up, modification of operating point, earth fault, (emergency) shut-downs (Nicolet et al. 2003). Particularly, start and stop cycles of Francis turbines runners are associated to transverse vibration, caused by high-frequency pressure fluctuations (irregular fluid flow, see Huth, 2005).

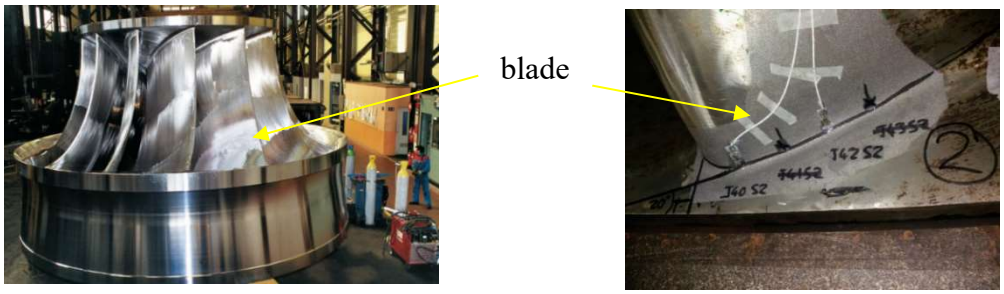

Fig. 1. Francis turbines: a) example of a runner ®EdF, b) welded joint of a blade (EdF & GE, 2018).

High-cycle fatigue (HCF) occurs, with associated deformation in every cycle remaining elastic, *i.e.* the maximum stress in the runner, denoted σ_{max}, remaining under the steel yield strength *YS* (Jabbado, 2006). Highest stresses usually appear at blade welds with the band and crown where each blade is fixed (Fig. 1). Figures 2 and 3 provide examples of strain histories in the cases of two different turbines (Francis Fig. 2 and Pelton Fig. 3). Figure 2 shows the turbine start (a) and stop (c) phases and the steady operating period (b) in the case of a Francis runner. Figure 3 also show examples of unsteady steady sequences, in the case of a Pelton runner. In such a figure, different strain evolutions can be observed for different power levels (Fig. 3a) and also for start and stop sequences, coupled with steady state sequences (Fig. 3b) and only used to help a pump to start ("back-to-back" start-ups, Fig. 3c).

These evolutions show very different unsteady behaviors. Figure 2 shows that the strain amplitude in steady state is less significant compared to a few seconds of start-up or shutdown, whereas Therefore Figure 2 seems to highlight that the cost of one hour in steady state is insignificant compared to a few seconds start-up or shutdown.

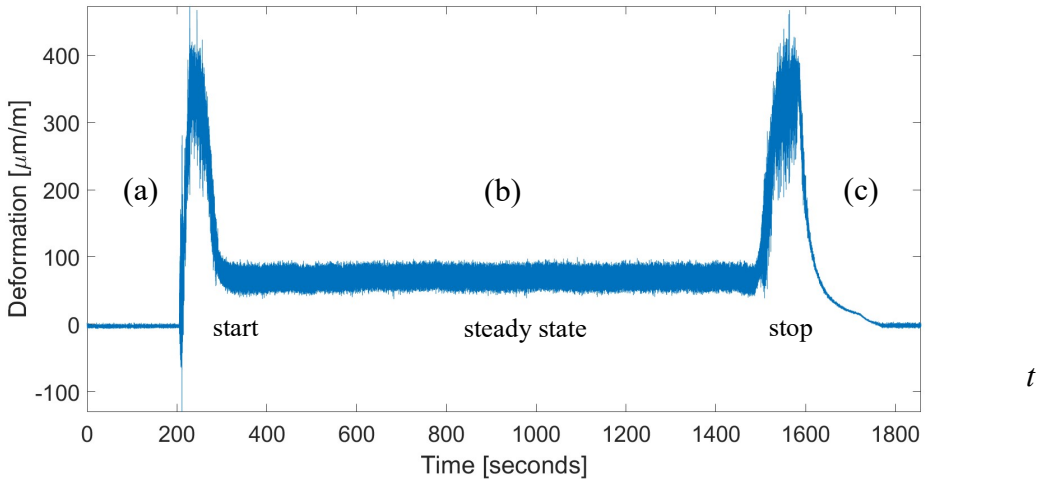

Fig. 2. Evolution of strain measurements for 3 loading sequences (Francis runner) ®EdF.

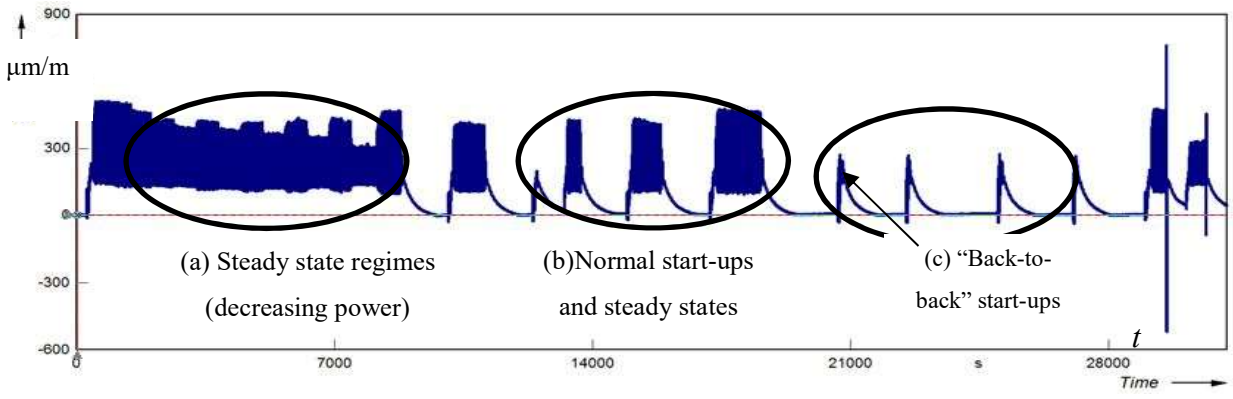

Fig. 3. Evolution of strain measurements for various loading sequences (Pelton runner) ®EdF.

On the contrary, Figure 3 displays steady states (with different power ranges) with comparable strain amplitudes compared with start-ups and shutdowns (Fig 3a).

In the last two figures, the strain gauges were positioned near the critical points ("hotspots"), where the stress values (von Mises) are the highest. In the case of a Francis runner (figure 2), they were located at the junction between blade and crown and at the junction between blade and band; the first was analyzed because of higher recorded values. In the case of a Pelton runner (figure 3), gauges were located at the bucket root.

The stress history can be deduced from such strain measurements from the gauge the closest to the zone with the maximum stress σ_{max} in the runner. Denoting σ_{nom} the nominal stress deduced from the gauge, one usually define the stress concentration factor K_t as the ratio between σ_{max} and σ_{nom}.

$$K_t = \frac{\sigma_{max}}{\sigma_{nom}} \quad \text{....(1)}$$

In Fig. 4, an example of a stress signal during a simplified start-up sequence is shown, highlighting stress HCF cycles. Meanwhile, the whole start-up operation can be considered as a low-cycle fatigue (LCF) cycle, as it occurs less than 10^6 times in the lifetime of the equipment. In this figure, stress amplitudes of HCF and LCF cycles are respectively denoted $\sigma_{a,HCF}$ and $\sigma_{a,LCF}$. The mean stress is denoted σ_m.

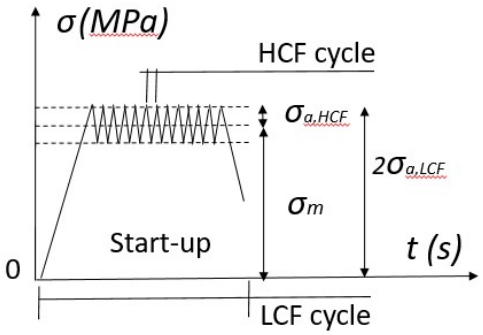

Fig. 4. Stress history highlighting a start-up sequence (runner scale).

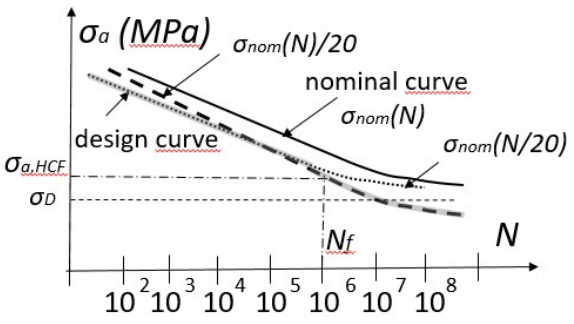

Fig. 5. *S-N* curve: nominal and design curves (laboratory specimen scale).

2.2 Fatigue assessment using regulatory or P-S-N Curves

Fatigue assessment of a runner usually consists in using a *S-N* curve, which is based on strain–controlled fatigue tests of small specimens at room temperature in air or in corrosive environment (see e.g. Buxbaum & Ostermann, 1983) or (Sonsino & Dieterich, 1990). Figure 5 displays a nominal *S-N* curve and the corresponding fatigue endurance limit (FEL) under which the stress amplitude σ_a will not lead to a failure, whatever the number N of cycles (see Lei et

al. 2021). Figure 5 also displays a design curve. For example, Figure 5 shows the regulatory number of cycles to failure N_f, related to the HCF stress amplitude $\sigma_{a,HCF}$.

The current nuclear design codes such as RCC-M (AFCEN, 2008) or ASME codes (Section III fatigue design curves, see Chopra & Shack 2003) define nominal curves as best–fit median curves to the experimental test data accounting for modifications (in particular but not only):

- to account for the effects of mean stress using the modified Goodman relationship

$$\sigma_{\text{nom}} = \sigma_a \left(1\text{-}\frac{\sigma_m}{UTS}\right) \ldots \textbf{(2)}$$

with UTS the ultimate strength of the runner material, σ_m the mean stress, σ_{nom} the nominal stress, and σ_a the applied stress amplitude (Pa).

- and then lowered by a factor γ_S of 2 on stress and γ_N of 20 on cycles to obtain the fatigue design curves.

$$\sigma_{\text{d}}\,(N) = \text{Min}[\sigma_{\text{nom}}(N)/2;\ \sigma_{\text{nom}}\left(\frac{N}{20}\right)] \ldots \textbf{(3)}$$

These passage factors (γ_S, γ_N) are supposed to cover conservatively two different effects: the variability of the lifetime under fatigue between laboratory tests and a structure within its real environment on the one hand, and between laboratory specimens on the other hand (Grandemange & Faidy, 2000), (Sudret, 2011). Chopra & Shack (2003) underlined that these factors are not safety margins but rather adjustment factors. They are not intended to address all the environmental effects on fatigue life. For example, fatigue data obtained in the U.S. and Japan demonstrate that light water reactor environments can have potentially significant effects on the fatigue resistance of steels, such that the current ASME Code design curve can become nonconservative for certain materials. Moreover, RCC-M or ASME codes seem rather to be validated for fatigue lives under $N = 10^5$ and $N = 10^6$ respectively. These last two limits of regulatory curves encourage to use probabilistic *S-N* curves (Balaji Rao et al. 2013, Fouchereau, 2014, Seddik, 2017). Indeed, *P-S-N* curves can correspond to a given probability to get a lower stress amplitude. Figure 6 depicts as an example a *P-S-N* curve based on the common assumption of a Gaussian probability law modelling the nominal stress.

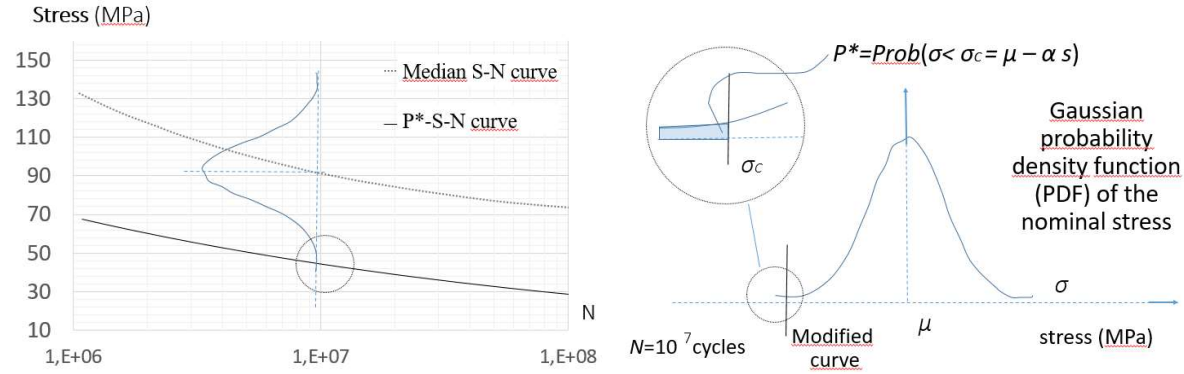

Fig. 6. Example of a design curve defined as a probabilistic *S-N* curve.

The position of the design curve therefore depends on the knowledge of a standard deviation s and a target probability P^*, defined in Eq. 5 (cf. Fig. 6 and Table 3).

Table 3

Target probability values P^* depending on α, such that $P^*=Prob(\sigma< \sigma_C = \mu - \alpha\, s)$.

Probabililty *P**	0.05	10^{-2}	10^{-3}	10^{-4}	10^{-5}
α	1.645	2.33	3.1	3.72	4.26

Passage factors (γ_S, γ_N) become finally particularly relevant if a corresponding *P-S-N* curve can be defined. For instance, the use of a characteristic value can be considered, as it is defined in design codes such as Eurocode (CEN, 2002). Particularly, a 5% characteristic value σ_k, associated to a partial safety coefficient γ, could be defined such as

$$\sigma_k = \sigma_m - 1.645\, s \quad \text{and} \quad P(\sigma < \sigma_k) = 0.05 \qquad \text{....(4)}$$

$$P^* = P(\sigma < \sigma_C = \sigma_k / \gamma) \qquad \text{....(5)}$$

2.3 The extra cost due to the increase of start and stop cycles

In the simplified case presented Fig. 4, there is only one HCF stress amplitude $\sigma_{a,HCF}$, for n_{HCF} cycles, and one LCF cycle with stress amplitude $\sigma_{a,LCF}$. Then the damage caused by these cycles can be written:

$$d = \frac{1}{N_f^{LCF}} + \frac{n_{HCF}}{N_f^{HCF}} \qquad \text{....(6)}$$

More realistically, an on-site stress history leads to a complex series of stress amplitudes (see Fig. 2 and 3). For such complex loading history, histograms of stress amplitudes can be extracted using a cycle-counting method such as rainflow method, Markov chain or ARMA model methods (Ling et al. 2011). Figure 7 displays simplified distributions of cycles obtained for the two damaging sequences of a Pelton turbine (Ballester 1992): full-power steady state

(Fig 7a, corresponding to Fig. 3b setting), and "back-to-back" start-up sequence (Fig. 7b, corresponding to Fig. 3c setting).

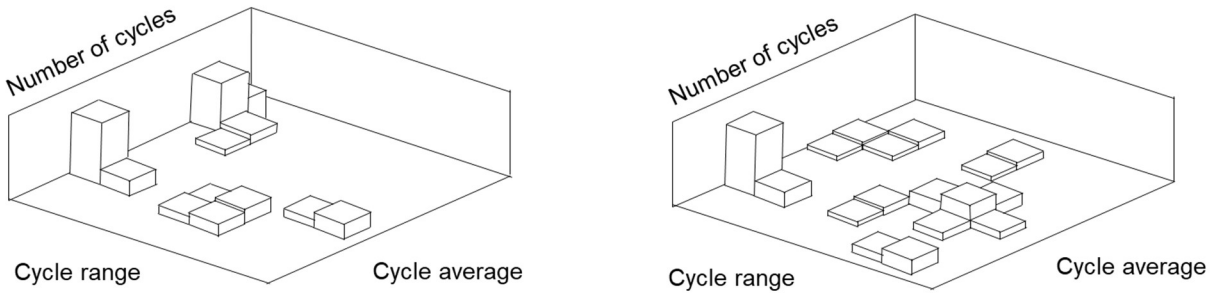

a) b)

Fig. 7. Simplified distributions of cycles extracted after a cycle-counting procedure: case (a) full-power steady state, and case (b) start-up sequence.

Damage corresponding to these cycles distributions is estimated using Palmgren-Miner's damage accumulation rule, summing elementary damages, more generally denoted n_j, such that

$$d = \sum_{j=1}^{r} \frac{n_j}{N_{f,j}} \qquad \text{....(7)}$$

The well-known cumulative damage method (EN 1993-1-9, 2005) means that a total damage is reached for d=1. However, such a rule does not help to estimate the lifetime of runners, given that this lifetime can be impacted by phenomena that cannot be measured using damage estimation.

In this paper, damage estimation principle only aims at comparing steady and unsteady sequences. The idea is to use cycle-counting to different sequences, then to extract damages and finally to compare them. Damage ratios could then help quantifying how start of stop sequences are more damaging (or not) compared to a supposed steady state.

The next section will present such an approach.

3 Estimation of damage ratios due to runners start and stop

This section presents how to estimate equivalent number of operating hours for start and stop events. Principle of this estimation is resumed in Fig. 8 and is explained. Then, a probabilistic *S-N* curve is determined, based on fatigue tests data.

3.1 Presentation of the approach

The proposed method consists first in the instrumentation of the runners with strain gages (Fig. 8a) (Lofflad et al. 2014). The question whether extensometers (unidimensional gages

instead of rosette gages) are sufficient has to be discussed. To do this, a finite element (FE) model can be used to estimate the stress concentration factor K_t (Bryla et al. 2013) and to confirm that uniaxial strain are representative of the real strain state (Morissette et al. 2016). These strains are derived after gages signal processing, accounting for a gauge factor and after filtering, accounting for signal noise (Fig. 8b). Finally, stresses are deduced by means of Hooke's law and Young's modulus of the runner E^{runner} and by checking that the maximum stress is below the yield strength *YS* (Fig. 8c). Loading sequences are selected for start and stop and steady states, with durations Δt_{st}, Δt_{sp}, Δt_{sy} (Fig. 8d). Then cycle counting allows obtaining stress amplitudes σ_a vs number of loading cycles n_j, for each sequence (Fig. 8e). A design curve is defined using *P-S-N* curves based on laboratory tests on specimens (Fig. 8f). As a consequence, Palmgren-Miner's damage accumulation rule leads to elementary damages d_{st}, d_{sp}, d_{sy} (Fig. 8g) and damage ratios d_{st}/d_{sy} and d_{sp}/d_{sy} (Fig. 8h) are deduced. Figure 8 summarizes the main steps of the approach.

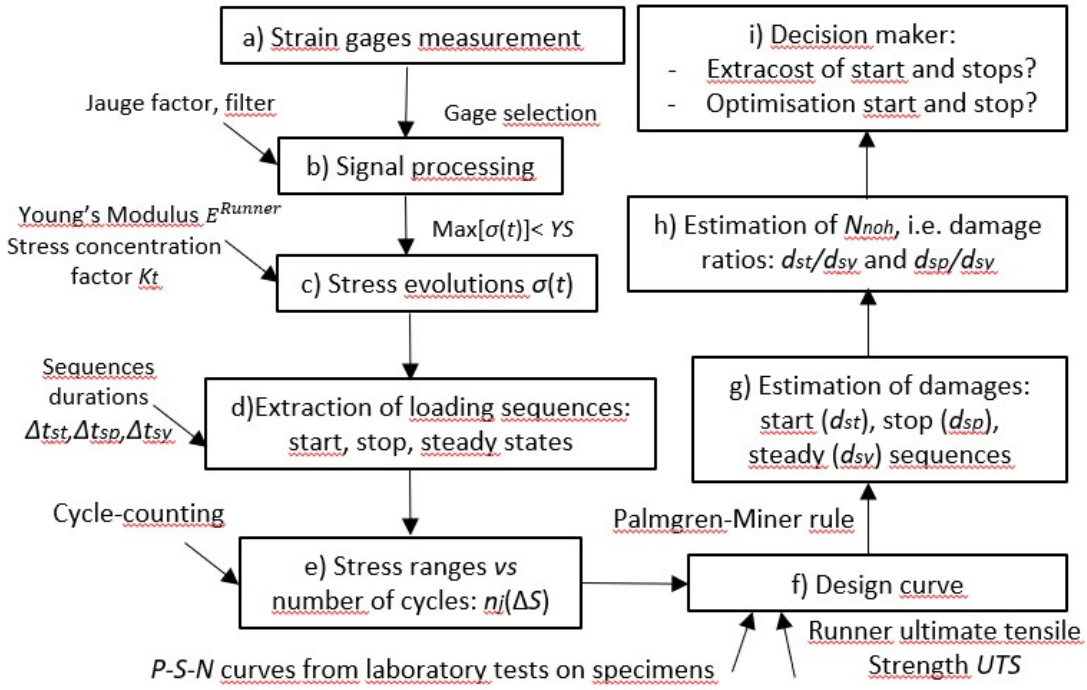

Fig. 8. Flowchart of the method estimating the numbers of normal operating hours N_{noh}.

From these damage ratios are derived: equivalent numbers N_{noh} of normal operating hours

$$N_{\mathrm{noh}}^{i} = \frac{\Delta t_{sy} d_i}{\Delta t_i d_{sy}} \quad \text{... (8)}$$

where (N_{noh}^{i}, Δt_i, d_i) denotes ($N_{\mathrm{noh}}^{\mathrm{st}}$, Δt_{st}, d_{st}) and ($N_{\mathrm{noh}}^{\mathrm{sp}}$, Δt_{sp}, d_{sp}) for start and stop transient sequences respectively.

Elementary damages d_{st}, d_{sp}, d_{sy}, denoted as d_j in the following, are the ratios between the numbers of loading cycles n_j and $N_{f,j}$. The number of cycles n_j is given by a cycle-counting

method (Fig. 8e). For example, Figure 9 displays distributions of elementary damage d, deduced from histograms (Fig. 7) and using numbers of cycles to failure $N_{f,j}$ estimated from a P^*=1/100 S-N curve (Ballester 1992).

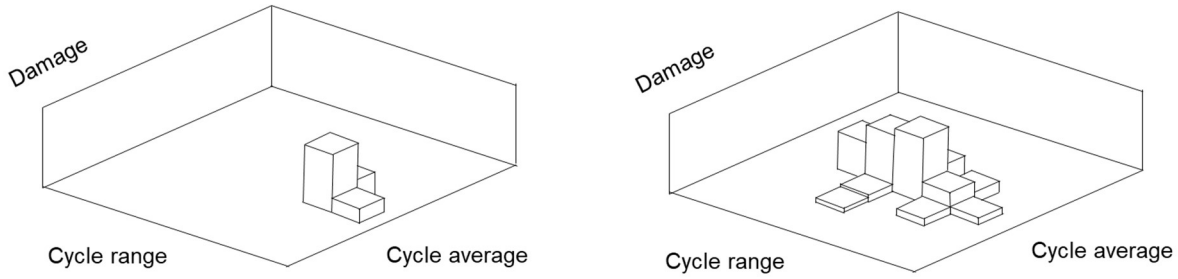

a) b)

Fig. 9. Simplified distributions of damage: case (a) full-power steady state, compared to start-up sequence case (b), with more cycles and cycle ranges, leading to more damage.

In the case of full-power steady state (Fig. 7bis a), most damaging cycles are those corresponding to the stresses after water impact: on the blades in the case of Francis runners, on the buckets in the case of Pelton runners. As an example, in the case of back-to-back start of a pump (Fig. 7bis b), Ballester (1992) estimated that the accumulation of damage of the Pelton runner leads to N_{noh} = 3 times the total damage found in case a).

The next section presents how to define the cycles number at failure Nf_j using a design curve, based both using probabilistic and regulatory S-N curves, as proposed.

3.2 Probabilistic *S*-*N* curves

This section is divided into three parts: i) the presentation of fatigue test series, ii) the modified Goodman relationship, taking into account the effect of mean stress, iii) the estimation of P-S-N curves in accordance with the design rules.

Fatigue test series

Series of tests were carried out on dozens of specimens, under axial and also combined axial and lateral cyclic loading, on 2 types of specimens and several steel grades (Buxbaum & Ostermann, 1983). These tests have been carried out in the same conditions as industrial runners. They are extracted from large-sized casted blocks. The size of the specimens is consistent with the dimensions of the runners. Only 13.4 steel with yield strength YS = 628 MPa and ultimate strength UTS = 804 MPa is used here. Figure 10 shows the two types of specimens, which correspond to:

- axial cyclic tests: the stress is assumed to be homogeneous in cross-section, which leads to a stress concentration factor K_t of 1;

- combined axial and lateral cyclic tests composed of notched prismatic specimens, with K_t equal theoretically to 1.36.

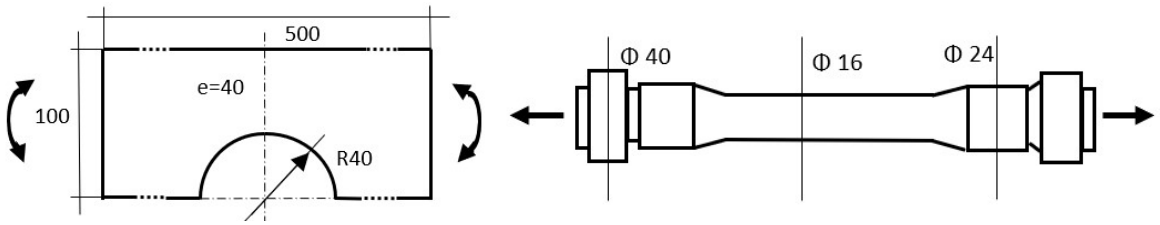

Fig. 10. Specimen under flexural bending (left) and tension (right) (Buxbaum & Ostermann, 1983), cf. Table 4

Table 4 gathers configurations depending on test conditions in air or in corrosive environment and on the zero mean stress levels (R=-1), equal to 204 MPa, or $\sigma_{nom}/2$ (R=0). For each combined axial and lateral cyclic test, stresses are deduced from measurements at the edge or center of the specimens (series 4b and 4c). A theoretical stress concentration factor K_t is given. In the following, we particularly study tests series 3 and 4, because they have been carried out in corrosive environment similar to the one of industrial runners.

Table 4
Synthesis of test series (Buxbaum & Ostermann, 1983), cf. Fig. 10.

Series d'essais	Environment corrosive	Type of mechanical loading	(Ratios of) stress min., moy. max.	Theorical stress concentration factor
0	air	Alternate tension	R = -1, $\sigma_m = \sigma_{nom}/2$	1
1	air	Alternate tension	R = 0, σ_{min}=0 MPa	1
3b (3c)	corrosive	Alternate bending	R = 0, σ_{min}=0 MPa	1.36 (1)
4b (4c)	corrosive	Alternate bending	σ_m=204 MPa	1.36 (1)

Table 5 presents some statistics on selected test series. The dispersion of the measurements is estimated by the coefficient of variation of the stress amplitude σ_a for N=10^7 cycles. Figure 11 also shows the dispersion of the measurements. This coefficient of variation fluctuates from about 10 to 20% depending on the series, with an increasing trend for higher mean stress.

Table 5
Stress amplitudes σ_a in cases of series 0, 1, 3, 4 (Buxbaum & Ostermann, 1983).

Tests series	Tests number	N variation domain Δ	Stress σ_a N=10^7(MPa)	Mean stress (MPa) (Standard deviation)	Coefficient of variation
0	15	$4.10^5 - 2{,}3.10^7$	182	32 (24)	0.21
1	18	$2.10^6 - 10^8$	110	13 (9)	0.14
3b	15	$1.610^6 - 10^8$	92	9 (8)	0.14
3c	8	$2.510^6 - 10^8$	74	5 (5)	0.11
4b	9	$6.10^5 - 10^8$	65	6 (4)	0.09
4c	14	$2.10^6 - 10^8$	52	6 (5)	0.16

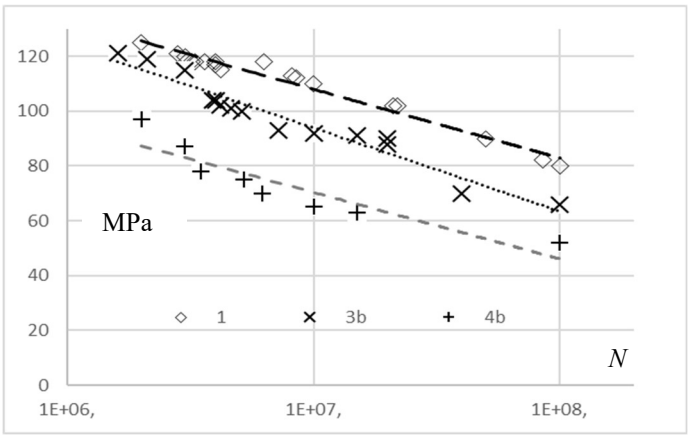

Fig. 11. Examples of measurements series (1, 3b et 4b) (Buxbaum & Ostermann, 1983), see. Table 3. Series correspond to tensile stresses (Fig. 10, right) and series (3b, 4b) to bending stresses (Fig. 10, left).

Accounting for the mean stress and stress concentration factor

Table 6 presents these modifications for $N = 10^7$ and 10^8 load cycles, in the case of series 3 and 4, with measurements at the edge and in the center of the specimens. Two types of modification can then be estimated:

- taking into account the mean stress: modified Goodman relationship, from 4 to 25%;
- the stress concentration factor K_t, estimated here between 1.23 and 1.4 (1.36 theoretically).

Table 6
Modified stress amplitudes (MPa) depending on the mean stress, for test series 3, 4 de (Buxbaum & Ostermann, 1983), 13.4 steel, ultimate limit strength of 804 MPa, from measurements at the edge and center of specimens

Specimen edge				Specimen center (close to the notch)				K_t tests
Series 3b (edge) and 3c (center) : case R=0, i.e. σ_{min}=0MPa and $\sigma_m = \sigma_a/2$								
	σ_a	Correct.(%)	σ_{nom}		σ_a	Correct.(%)	σ_{nom}	
$N = 10^7$	72	4.5	75	$N = 10^7$	59	3.7	61.2	1.23
$N = 10^8$	90	5.6	95	$N = 10^8$	74	4.6	77.6	1.23
Series 4b (edge) and 4c (center): case σ_m =204 MPa								
	σ_a	Correct.(%)	σ_{nom}		σ_a	Correct.(%)	σ_{nom}	
$N = 10^7$	52	25.4	70	$N = 10^7$	37	25.4	49.6	1.41
$N = 10^8$	70	25.4	94	$N = 10^8$	54	25.4	72.4	1.30

The stress concentration factor of 1.36 is not exactly found, partly because of the uncertainties in the stress estimate and partly because it seems unlikely that the maximum stress was accurately measured at the center of the specimens. For safety reasons, K_t = 1.36 will be considered in the following.

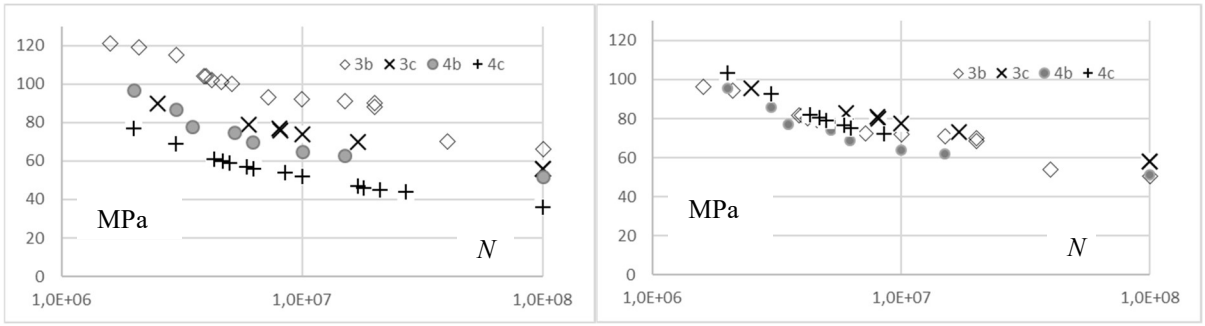

a) before Goodman modifications b) after Goodman modifications (see Eq. 2)

Fig. 12. Mean *S-N* curves (13.4 steel), series 3b, 3c, 4b, 4c

Looking for nominal and design *S-N* curves

In order to carry out a fatigue design, it is necessary to define a nominal curve, which can in principle be deduced from each of the 4 above-mentioned curves. Figures 12a and 12b show the mean Wöhler curves of series 3 and 4, derived from measurements at the edge and center of the specimens, before and after Goodman modifications. If we do not use the mean curves, but all the stress amplitudes, we obtain an average dispersion of 13%, which is the average coefficient of variation that can be deduced from Table 3. Defining a nominal curve could then consist of a regression of one curve among others or of the mean points of Fig. 12b. Equation 9 provides the equation of the regression for all series 3 and 4.

$$\sigma_{\text{nom}} = -10.66\,\text{Ln}(N) + 245.19 \ldots \textbf{(9)}$$

This 50% *S-N* curve is plotted on Fig. 13., with different corrected design curves. Indeed, one considers at least three options:

- a) a *P-S-N* curve; Figure 13a proposes 0.1% and 0.01% *S-N* curves, deduced from the 50% *S-N* curve (Eq. 8), and following Table 1 and Eqs. 4-5;
- b) a regulatory curve deduced from the 50% *S-N* curve (Eq. 8), applying the design rule (Eq. 3); Figure 13a shows that this curve is very close to the 0.01% *S-N* curve;
- c) regulatory curves deduced from the design code (ASME, 2013).

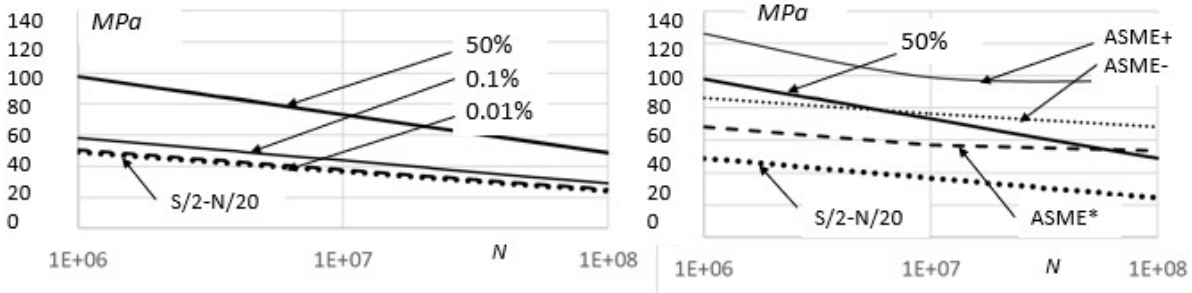

a) Mean regression curve σ_a, P=10^{-2} and10^{-4} *S-N* curves and corrected *S-N* curve according to (AFCEN, 2008), (Chopra & Shack, 2003)

b) Nominal curves for highly and poorly alloyed steel (ASME, 2013), compared with other curves

Fig. 13. Corrected design S-N curves deduced from the mean experimental series (a), from ASME code (b).

Last option, c) curves denoted ASME+ and ASME-, respectively, correspond to carbon and low-alloy steels (Young's modulus E of 206.8 GPa) and austenitic stainless steels (E = 195.1 GPa) (ASME, 2013). Contrary to *P-S-N* curves deduced from the presented experimental series, ASME *S-N* curves do not account for any corrosive environment, justifying arbitrarily corrected *S-N* curve by dividing nominal stress values by a safety factor, e.g. 1.5 (see Brand et al., 1999). Therefore Figure 13b shows the revised *S-N* curve, denoted ASME*, accounting for this coefficient and also ~~a~~ 200 GPa Young's modulus. It is worth noting that if this revised curve is conservative for $N < 10^7$, it becomes far less conservative for larger number of cycles, which corroborates the analysis found in Chopra & Shack (2003), in the case of a usual fatigue assessment.

4 Application to Francis and Pelton runners

Method presented in the section 2 is applied here to Francis and Pelton runners. Considered runners are listed in Table 7. They are all made using 13.4 steel, with Young's modulus of 200 GPa. Signal filtering and cycle counting are applied in four cases, before estimating damage ratios, i.e. equivalent number of normal operating hours. For all studies, signals were acquired at a 2400 Hz frequency with an anti-aliasing filter.

Table 7

List of runners (EdF fleet of hydroelectric power plants).

	Runner type	**Effective power**
Runner 1	Francis (turbine)	28 MW
Runner 2	Francis (turbine)	2 MW
Runner 3	Pelton (turbine)	> 80MW
Runner 4	Pelton (Ballester, 1992)	152 MW

4.1 Case of a 28 MW Francis runner (runner 1)

This runner has been studied estimating a maximum stress of 60 MPa (EdF & GE, 2018), for an estimated maximum deformation of 300 μm/m. However, the maximum deformation found (J1S8 gauge) is 132.5 μm/m, which leads us to consider a stress concentration factor K_t of 2.27 with an accuracy of about 3% (K_t estimated between 2.16 and 2.34, EdF & GE, 2018). For the power of 28 MW, K_t = 2.16~~,~~ is the coefficient we propose to consider in the following.

Signal filtering and cycle-counting

A spectral analysis is performed to quantify the impact of all degradation phenomena occurring at the runner, and determine the filter to be applied to separate the real effects from the signal noise. Fast Fourier Transform was performed during 5 minutes-long stabilized operating signal (Fig. 14). The eigen frequency $F_0 = n_o/60 = 2.63$ Hz directly depends on the rotational frequency of the runner, where $n_0 = 158$ rpm is the rated synchronous speed of the runner.

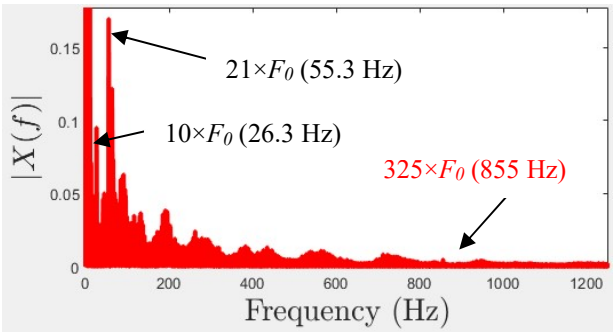

Fig. 14. Spectral analysis of the signal using a fast Fourier transform (FFT): evolution FT modulus vs frequency.

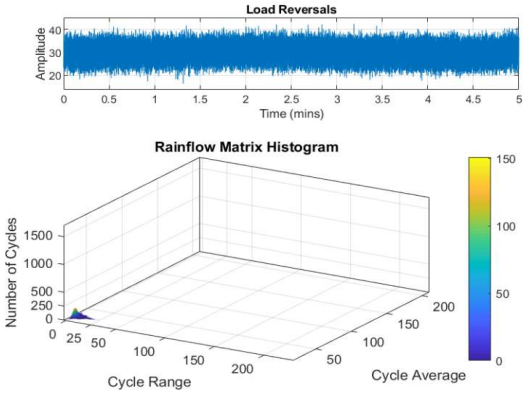

Fig. 15. Representation of the rainflow counting matrix using loading history of a steady regime.

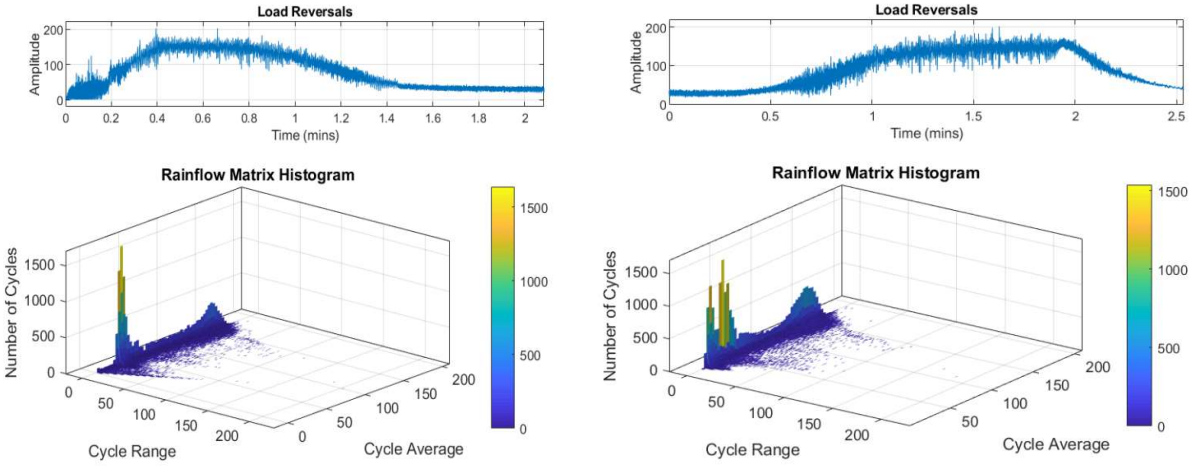

Fig. 16. Representation of the rainflow counting matrix using a load history data in case of 28 MW startup (a) and stop sequences (b) (Runner 1).

The analysis shows harmonics at $2\times F_0$, $3\times F_0$ up to $21\times F_0$, with a natural frequency F_0 equal to 2.63 Hz. The harmonics captured in the spectrum could probably correspond to hydraulic instabilities e.g. to the Zr =13 blades ($Zr\ F_0$ = 34.2 Hz), to the Zs = 24 wicket gates ($Zs\ F_0$ = 63.2 Hz)). The value of 855 Hz is an example that corresponds in fact to 25 $Zr\ F_0$, harmonic of the interaction between the stationary pressure field (on the distributor side) and a rotating pressure field - (on the runner side)). At 55.3 Hz is detected the rotor-stator interaction and at 26.3 Hz interblades vortexes.

The 1 kHz filter is eventually applied in the following, given that ISO 20816-5 (2018) also recommends ~~not~~ filtering not below 1 kHz.

Rainflow counting algorithm (ASTM, 2011) is used to translate time-dependant stress loading into stress cycles amplitudes. For illustration, Figure 15 displays the steady state regime during Δt_{sy} = 5 minutes, for a power stabilized at 28 MW, and a representation of the rainflow counting matrix, with histograms depending on amplitude (cycle range), mean stress (cycle average) and number of cycles.

Figures 16 represent the rainflow counting matrix using a load history data in the same case of a 28 MW start-up (a) and shutdown sequences (b). Their durations are respectively equal to Δt_{st} = 2 min and Δt_{sp} = 2.5 min. On the histogram, fairly high numbers of cycles are reported compared to steady state sequence, where average cycles clearly less than 50 MPa.

Estimations of damage and normal operating hours

From this last observation, it seems irrelevant to account for an endurance limit. This can be checked displaying damage estimations for steady, start and stop sequences, with and without 30 MPa fatigue endurance limit (FEL). This comparison is proposed in Fig. 17, accounting for arbitrarily FEL = 30 MPa, using ASME* (a) and P=10^{-4} (b) S-N curves respectively. This figure highlights that the steady regime corresponds to stress amplitude mostly lower than the FEL. As a consequence, normal operating hours estimated in Tab. 6 increase drastically.

a) ASME* S-N curve b) P=0.1% S-N curve

Fig. 17. Representation of damage estimations for steady, start and stop sequences, with and without 30 MPa endurance limit, accounting for ASME* (a) and P=10^{-4} (b) S-N curves respectively (runner 1).

Table 8 gathers estimations of normal operating hours (N_{noh}, defined in Eq. 8) obtained for runner 1, in cases of start and stop events. Three design curves presented in section 3 (Fig. 13) have been used to estimate damage ratios, considered as N_{noh} estimations for these events (Fig. 16). For example, the first column provides the damage ratio (extracost) of a start-up, using the ASME* curve (Fig. 13b), without accounting for a fatigue endurance limit (FEL). It means that stress amplitudes below the FEL have been ignored to estimate elementary damages.

Table 8

Number of normal operating hours (N_{noh}), start-up of the 28 MW Francis (runner 1)

Sequence	*ASME**	*ASME**	*P=0.1%*	*P=0.1%*	*P=0.01%*
(with/without FEL)	*without*	*with*	*without*	*with*	*without*
Start-up	6	51	13	141	658
Stop	6	78	12	205	423

Results from Table 8 seems conservative to account for the FEL. Anyhow, since most stress amplitudes of steady regime sequence being below the FEL, the operator better should consider them. Table 8 also shows that estimations of extra cost of start and stops highly depend on the choice of the *P-S-N* curve: N_{noh} increases as *P* decreases. For example, N_{noh}=141h means that a start-up corresponds to 141h of normal operating hours if we consider a *P-S-N* design curve with *P*=0.1% and if we account for the FEL in the estimation of the damage ratio N_{noh}. Moreover, runners' operator should bear in mind that *P-S-N* curves are estimated from a limited number of tests, between $N=10^6$ and 10^8 cycles, whereas damage estimation needs to use *S-N* curves for higher N values. This last observation would then tend to recommend a regulatory curve such as ASME ones, defined to $N=10^6$ cycles. The operator has finally to choose a safety factor, arbitrarily equal to 1.5 in this work, but which should probably be taken larger.

4.2 Other runners and discussion

This section gathers results obtained using other runners (Tab. 5).

Runner 2 (2 MW Francis turbine)

This study was conducted using histories observed working on a runner similar to runner 1. We consider the same material and also the same stress concentration factor. For technical reasons, we were only able to focus on a start-up of 2 MW. Figure 18 represents histograms of a start-up (a) and the steady state regime (b). In this case, a startup of less than 2 minutes corresponds to around 35 minutes of steady regime, using the *P*=1% *S-N* curve.

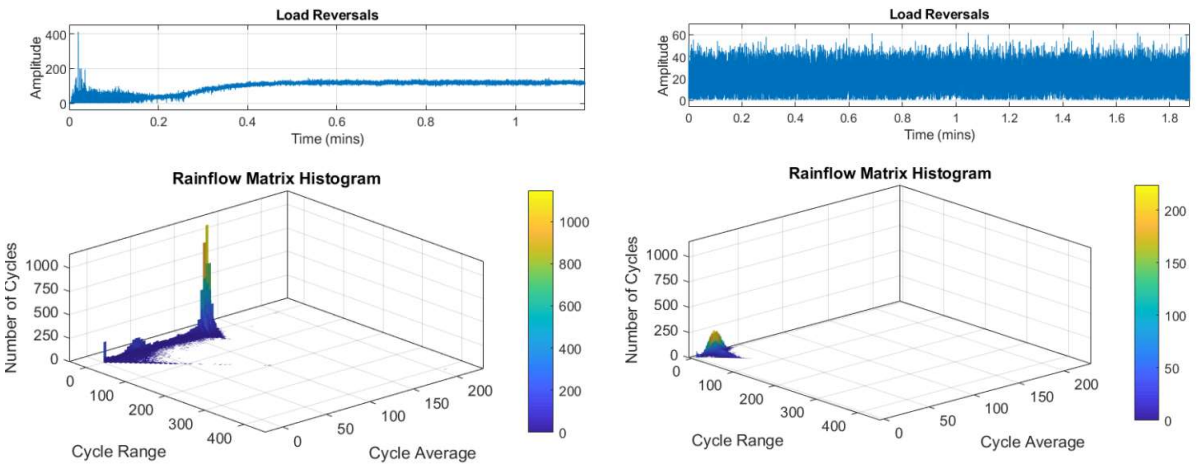

Fig. 18. Representation of the rainflow counting matrix for a Francis turbine in case of 2 MW startup (a) and steady regime (b) (runner 2)

Pelton runners 3 and 4

Considered Pelton runners 3 and 4 are used to start a reversible machine in pump mode. Runner 3, with power greater than 80 MW, can be used to start a turbine-pump less powerful. In this case, there is clearly no extra cost due to start or stop.

Runner 4 has the same power as the turbine-pump to be started (Ballester 1992). In this case, the start-up of this runner is equivalent to 3 normal operating hours.

5 Conclusion

The paper presents a strategy to estimate the extra cost of start and stop of hydro turbines, under high-cycle fatigue. The method compares estimations of cumulated damages from three elementary sequences representing steady and transient regimes (start and stop cycles) of turbine runners. These estimations are based on regulatory or probabilistic *S-N* curves, determined using fatigue tests data. The approach has been applied to Francis runners, using also a past result on a Pelton runner, published only in French (Ballester 1992).

The proposed approach is interesting to detect and quantify extra cost of start and stop in terms of normal operating hours. However the operator has to bear in mind that these estimations depend on the reference *S-N* curve used to estimate elementary damages. Laboratory tests or regulatory curves are useful, but one has to use them with caution. For example, one of the available ASME curves was designed for austenitic steel used in nuclear industry, but not used for runners of hydraulic plants.

Once an extra cost has been detected, the recommendation from Gagnon et al. (2010) can then be followed if possible, i.e. optimize this start-up scheme with regard to fatigue damage, in order to extend Francis runner life expectancy.

As perspectives, this approach could be applied to other ageing components such as penstock, or main shut-off valve. Ling et al. 2011 experienced to implement Markow chain or ARMA model method instead of rainflow cycle-counting method, that could also be improved (Anthes, 1997, Yung-Li et al. 2012).

Acknowledgements

The authors would also like to thank Philippe Bryla, Stéphan Courtin, Nicolas Dutruel, Thibaut Autrusson, for their scientific advices.

6 References

AFCEN (2008): RCC-M - Edition 2007 – Addendum dec. 2008: Design and Construction Rules for Mechanical Components of PWR Nuclear Islands.

Amzallag, C., Gerey, J.P, Robert, J.L. and Bahuaud J., « Standardisation of the rainflow counting method for fatigue analysis », Int. J of Fatigue, Vol 16(4), 287-293, 1994.

Anthes R. J.. Modified rainflow counting keeping the load sequence. Int. J. of Fatigue, 19(7) :529—535, 1997.

Arsić, M., Karić, R., Sedmak, A., Burzić, M. and Vistać B., Methodological Approach to Integrity Assessment and Service Life of Rotating Equipment at Hydropower Plant – Turbine Shaft, Structural Integrity and Life, Vol.13, No.2, 2013, 117–124.

ASME, American Society of Mechanical Engineers Boiler and Pressure Vessel Code (ASME Code), Appendix I to Section III, “Rules for Construction of Nuclear Facility Components”, 2013.

ASTM E1049-85(2017), "Standard Practices for Cycle Counting in Fatigue Analysis." West Conshohocken, PA: ASTM International, 2011.

Ballester, J.L. « Contribution to the study of the ageing of Pelton wheels: comparative damage ratios » (in French). Internal report EdF DTG MPSH, D.4100/EHM-G-92/08, 1992.

Bakken, B.H., (2002). Hydro unit startup costs and their impact on the short term scheduling strategies of swedish power producers. IEEE Power Engineering Society Summer Meeting.

Bakken B.H., Bjørkvoll T., « Hydropower Unit Start-up Costs », IEEE, 2002.

Balaji Rao, K., Anoop, M.B., Raghava, G., Prakash, M. and Rajadurai, A., Probabilistic fatigue life analysis of welded steel plate railway bridge girders using S-N curve approach. 2013, Proceedings of the Institution of Mechanical Engineers, Part O: Journal of Risk and Reliability 227: 385

Bureau of Reclamation, Hydrogenerator Start / Stop Cost, US 2014.

Brand, A., Flavenot J. F.; Gregoire R. and Tournier C., Technological data on fatigue, Senlis, CETIM, 1999, 4^{e} ed., 383 p. (in French).

Bryla, P., Pillou, M. and Bennebach, M., Operation of the Bois plant hydraulic turbine in bypass operating mode: analysis of the fatigue behavior, Procedia Engrg 66 (2013), 413-450.

Buxbaum, O. & Ostermann, H. Ausfallsichere Bemessung von Laufrädern für Wasserkraftmaschinen aus rostfreiem Stahlguss unter Berücksichtigung von Korrosion und Gefügezustand, Fraunhofer Institute for Structural Durability, Darmstadt, Germany, 1983. (Technical report in German)

CEN, 2002. Eurocode 0. Bases of Structural Design. Brussels: CEN.

Chopra, O.K. & Shack, W.J., Argonne National Laboratory, Review of the Margins for ASME Code Fatigue Design Curve - Effects of Surface Roughness and Material Variability. U.S. Nuclear Regulatory Commission Office of Nuclear Regulatory Research Washington, DC 20555-0001, 2003.

561 Dojčinović, M., Arsić, M., Bošnjak, S., Murariu, A. and Malešević Z., Cavitation resistance of turbine
562 runner blades at the hydropower plant 'DJERDAP', Structural Integrity and Life, Vol.17(1), 2017,
563 55–60.
564 Dorji, U. & Ghomashchi, R. « Hydro turbine failure mechanisms: An overview », Engineering failure
565 analysis 44 (2014) 136–147, Elsevier, 2014.
566 EN 1993-1-9 (2005): Eurocode 3: Design of steel structures - Part 1-9: Fatigue [Authority: The European
567 Union Per Regulation 305/2011, Directive 98/34/EC, Directive 2004/18/EC].
568 EdF & GE, « Prototype Air Injection Tests », confidential report, 2018
569 Fouchereau, R., Probabilistic modelling of S-N curves, PhD thesis, University Paris-Sud, 2014. (in
570 French)
571 Gagnon, M., Tahan, S. A., Bocher, P. and Thibault, D. « Impact of start-up scheme on Francis runner
572 life expectancy » 25th Iahr Symposium on Hydraulic Machinery and Systems, Iop Conf. Series :
573 Earth and Environmental Science 12 (2010) 012107
574 Gagnon, M., Tahan, S. A., Bocher, P. and Thibault, D. « A probabilistic model for the onset of High
575 Cycle Fatigue (HCF) crack propagation: Application to hydroelectric turbine runner » Int. J. Fatigue
576 47 (2013) 300–307.
577 Gagnon, M., Thibault, D. and Blain, M., « On the expected monetary value of hydroelectric turbine
578 start-up protocol optimisation », 13th world congress on Engrg Asset Managt, WCEAM, 2018.
579 Grandemange, J-M, Faidy C., General approach to preventing the risk of fatigue damage to nuclear
580 boiler equipment: from design to monitoring during operation SFEN-ST2 Day "Fatigue damage to
581 nuclear installations", Paris, 23 November 2000 (in French)
582 Hassanipour, M, Y. Verreman, Y., Lanteigne, J. and Chen J., (2015) Effect of Periodic Underloads on
583 Fatigue Crack Growth in Three Steels Used in Hydraulic Turbine Runners, Int. J. of Fatigue 85,
584 DOI: 10.1016/j.ijfatigue.2015.11.027
585 Huth, H-J, Fatigue Design of Hydraulic Turbine Runners, Doctoral thesis, Fakultet for
586 ingeniørvitenskap og teknologi, 2005
587 ISO 20816-5:2018 Mechanical vibration — Measurement and evaluation of machine vibration — Part
588 5: Machine sets in hydraulic power generating and pump-storage plants (2018)
589 Jabbado, M. Polycyclic fatigue of steel structures: life under varying loads. Mechanics of materials
590 Doctoral thesis of the Ecole Polytechnique, 2006 (In French)
591 Jacquemoud, R. "Towards a reliable operating range for a Kaplan turbine, beyond the guaranteed range,
592 based accounting for material fatigue damage processes", XVII IA HR symposium, Beijing, China
593 1994. (in French)
594 Kokko, V. (2014). Ageing due to start-stop cycles and frequent regulation in lifetime estimation of hydro
595 turbines and generators. SHF, Grenoble.
596 Lei, X., Yuan, L., Peng, L., Sun, C., Wei, B. and Wei Y., Fatigue endurance limit and crack front
597 evolution in metallic glass, Int. J. Fatigue 143 (2021) 106004.
598 Ling, Y., Shantz, C., Mahadevan, S. and Sankararaman, S., 2011. Stochastic prediction of fatigue
599 loading using real-time monitoring data. International Journal of Fatigue 33, 868–879.
600 https://doi.org/10.1016/j.ijfatigue.2011.01.015
601 Liu, X., Luo, Y. and Wang Z., A review on fatigue damage mechanism in hydroturbines, Renewable
602 and Sustainable Energy Reviews 54(2016), 1–14.
603 Lofflad J., Eissner M. and Graf B. « Strain Gauge measurements of rotating parts with telemetry » 9th
604 International Conference on Hydraulic Efficency Measurements, Trondheim, 2014.
605 Luna-Ramírez A., Campos-Amezcua A., Dorantes-Gómez O., Mazur-Czerwiec Z., Muñoz-Quezada R.,
606 Failure analysis of runner blades in a Francis hydraulic turbine — Case study, Engineering Failure
607 Analysis, Vol. 59, 2016, pp 314-325. https://doi.org/10.1016/j.engfailanal.2015.10.020
608 Marcouiller, L. & Thibault, D. « Obtaining stress measurements on runners as a key contribution to
609 reducing their degradation and improving the reliability of hydroelectric production units » HYDRO
610 conference, Bordeaux, 2015.
611 Matsuishi, M. & Endo, T. (1969), « Fatigue of metals subjected to varying stress », In *Proceedings of*
612 *the Kyushu Branch of Japan Soc. of Mech. Engrg,* Fukuoka, Japan (in Japanese), 37-40.
613 Mjølsnes, J. "Frequent Start/Stop. Costs for Hydropower Generators," Statkraft Engineering, Report
614 99/87, Sept. 1999 (in Norwegian).

615 Morissette, J.F., Chamberland-Lauzon J., Nennemann B., Monette C., Giroux A.M., Coutu A. and
616 Nicolle J., Stress predictions in a Francis turbine at no-load operating regime, 28th IAHR symposium
617 on Hydraulic Machinery and Systems, 2016, doi:10.1088/1755-1315/49/7/072016
618 Nicolet, C., Avellan, F., Allenbach, P., Sapin, A., Simond, J.-J., Kvicinsky, S., and Crahan, M.
619 Simulation of transient phenomena in Francis turbine power plants: hydroelectric interaction, 1–12.
620 13th conference on Waterpower, July 29–31, 2003 in Buffalo, New York, USA.
621 Nilsson, O. & Sjelvgren, D. (1997). Hydropower unit startup costs. IEEE Transactions on Power
622 Systems.
623 Savin, O., Badina, C., Baroth, J., Charbonnier, S. and Bérenguer, C., Start and stop costs for hydro
624 power plants: a critical review, Proc. of the 30th Europ. Safety and Reliability Conf. & the 15th Prob.
625 Safety Assessment and Management Conf., 2020.
626 Schijve, J., Statistical distribution functions and fatigue of structures, Int. J. Fatigue 27 (2005) 1031–
627 1039.
628 Seddik, R., Ben Sghaier, R., Atig, A. and Fathallah, R., Fatigue reliability prediction of metallic shot
629 peened-parts based on Wöhler curve, Journal of Constructional Steel Research 130 (2017) 222–233
630 Sonsino, C.M. & Dieterich, K., Fatigue strength of steel types G‐X5CrNi 13 4 and G‐X5CrNi 17 4
631 used for blades of water‐power turbines and pumps, Werkstoffe und Korrosion 41, 330-342, 1990.
632 Sudret, B. (2011). Probabilistic design of structures submitted to fatigue, Fatigue of materials and
633 structures, chapter 5 (C. Bathias and A. Pineau (Eds)), 223_263. Wiley & Sons.
634 Susmel, L. Modified Wöhler Curve Method, theory of critical distances and Eurocode 3: a novel
635 engineering procedure to predict the lifetime of steel welded joints subjected to both uniaxial and
636 multiaxial fatigue loading. Int J Fatigue 2008; 30: 888–907.
637 Susmel, L. The Modified Wöhler Curve Method calibrated by using standard fatigue curves and applied
638 in conjunction with the theory of critical distances to estimate fatigue lifetime of aluminium
639 weldments. Int. J. Fatigue 2009; 31: 197–212.
640 Yung-Li, Lee, Y.-L. and Tjhung, T. A new definition of the rainflow cycle counting method, Metal
641 Fatigue Analysis Handbook, 89-114, 2012.
642 Welte, T. Deterioration and maintenance models for components in hydropower plants, Doctoral thesis,
643 Norwegian University of Science and Technology (NTNU), 2008.
644 Wöhler, A., 1860. Versuche zur Ermittlung der auf die Eisenbahnwagenachsen einwirkenden Kräfte
645 und die Widerstands higkeit der Wagen-Achsen. Zitschrift für Bauwesen, Vol. 10, 583- 616. (In
646 German).
647